Geophysical Research Letters

RESEARCH LETTER
10.1029/2024GL109893

A Mechanism for Ice Layer Formation in Glacial Firn

Mohammad Afzal Shadab[1,2,3,4], **Surendra Adhikari**[4], **Anja Rutishauser**[5], **Cyril Grima**[2,3,6], **and Marc Andre Hesse**[1,3,6]

[1]Oden Institute for Computational Engineering and Sciences, The University of Texas at Austin, Austin, TX, USA, [2]University of Texas Institute for Geophysics, The University of Texas at Austin, Austin, TX, USA, [3]Center for Planetary Systems Habitability, The University of Texas at Austin, Austin, TX, USA, [4]Jet Propulsion Laboratory, California Institute of Technology, Pasadena, CA, USA, [5]Department of Glaciology and Climate, Geological Survey of Denmark and Greenland, København, Denmark, [6]Department of Earth and Planetary Sciences, The University of Texas at Austin, Austin, TX, USA

Abstract There is ample evidence for ice layers and lenses within glacial firn. The standard model for ice layer formation localizes the refreezing by perching of meltwater on pre-existing discontinuities. Here we argue that even extreme melting events provide insufficient flux for this mechanism. Using a thermomechanical model we demonstrate a different mechanism of ice layer formation. After a melting event when the drying front catches up with the wetting front and arrests melt percolation, conductive heat loss freezes the remaining melt in place to form an ice layer. This model reproduces the depth of a new ice layer at the Dye-2 site in Greenland. It provides a deeper insight into the interpretation of firn stratigraphy and past climate variability. It also improves the simulation of firn densification processes, a key source of uncertainty in assessing and attributing ice sheet mass balance based on satellite altimetry and gravimetry data.

Plain Language Summary Firn covers a significant portion of Earth's glaciers and ice sheets. It can store surface meltwater and prevent runoff into the ocean. The widespread presence of ice layers embedded in firn formed by meltwater refreezing may prevent meltwater storage and contribute to sea level rise. However, current models of ice layer formation, originally developed for snow, do not seem to work in firn. This work presents a different mechanism for ice layer formation without invoking pre-existing ice layers within the firn. Our model shows that the sequencing of ice layers formed by subsequent melting events depends on the overall heat added to the firn. Deeper layers occur in warmer, more porous firn during intense melt events in a warming climate. This insight enhances our understanding of firn layering and can help deduce past climate variations. Our model aids in understanding the density evolution of firn to reduce uncertainties in remote sensing data that determines the ice sheet mass loss and its contribution to global sea-level rise.

Key Points:

- A new ice layer forms without meltwater perching when freezing localizes after a melt event as heat conduction dominates over advection
- Deeper ice layers form in warming climatic conditions whereas denser ice layers form near surface in net-zero climatic conditions
- Results indicate the possibility of deducing past variability in climate from firn stratigraphy and vice versa

Supporting Information:

Supporting Information may be found in the online version of this article.

Correspondence to:

M. A. Shadab,
mashadab@utexas.edu

Citation:

Shadab, M. A., Adhikari, S., Rutishauser, A., Grima, C., & Hesse, M. A. (2024). A mechanism for ice layer formation in glacial firn. *Geophysical Research Letters*, *51*, e2024GL109893. https://doi.org/10.1029/2024GL109893

Received 21 APR 2024
Accepted 16 JUL 2024

Author Contributions:

Conceptualization: Mohammad Afzal Shadab, Surendra Adhikari, Anja Rutishauser, Cyril Grima, Marc Andre Hesse
Data curation: Mohammad Afzal Shadab
Formal analysis: Mohammad Afzal Shadab, Surendra Adhikari, Anja Rutishauser, Cyril Grima, Marc Andre Hesse
Funding acquisition: Mohammad Afzal Shadab, Surendra Adhikari, Cyril Grima, Marc Andre Hesse
Investigation: Mohammad Afzal Shadab, Surendra Adhikari, Anja Rutishauser, Cyril Grima, Marc Andre Hesse
Methodology: Mohammad Afzal Shadab, Marc Andre Hesse
Project administration: Mohammad Afzal Shadab, Marc Andre Hesse

1. Introduction

Earth's glaciers and ice sheets are losing mass at unprecedented rates, significantly contributing to global sea level rise (Velicogna et al., 2020; Team-IMBIE, 2018; Mouginot et al., 2019; Zemp et al., 2019). Over the past few decades, polar ice sheets have experienced an increased intensity and spatial extent of surface melting (Bell et al., 2018; Horlings et al., 2022; Van Angelen et al., 2013). Approximately half of the Greenland Ice Sheet's annual mass loss is attributed to surface melting and runoff (Machguth et al., 2016; Van den Broeke et al., 2009). In high-elevation areas covered by firn (sintered and compacted snow), surface meltwater percolates down into the firn and refreezes to form ice layers (de la Peña et al., 2015; Harper et al., 2012a), shown in Figure 1. While percolation and refreezing processes buffer a significant amount of meltwater (Van Angelen et al., 2013), the firn's buffering capacity will eventually diminish as the pore space will increasingly reduce under future warming scenarios (Brils et al., 2024; Noël et al., 2017; Pfeffer et al., 1991; Van Angelen et al., 2013).

Remote sensing and in-situ measurements have confirmed the widespread presence of ice layers in Greenland (Culberg et al., 2021; Jullien et al., 2023; MacFerrin et al., 2019; Machguth et al., 2016; Samimi et al., 2020; Van den Broeke et al., 2009), the Canadian Arctic (Chan et al., 2022; Gascon et al., 2013; Rutishauser et al., 2016), and Antarctica (Alley et al., 2018; Jiahong et al., 1998; Kaczmarska et al., 2006). These ice layers may lead to perched water tables and lateral meltwater routing in the firn (de la Peña et al., 2015; Jullien et al., 2023; Machguth et al., 2016), amplifying the ice sheet mass loss into the oceans (Harper et al., 2012b; Machguth et al., 2016).

Resources: Mohammad Afzal Shadab, Marc Andre Hesse
Software: Mohammad Afzal Shadab
Supervision: Surendra Adhikari, Cyril Grima, Marc Andre Hesse
Validation: Mohammad Afzal Shadab
Visualization: Mohammad Afzal Shadab
Writing – original draft: Mohammad Afzal Shadab
Writing – review & editing: Mohammad Afzal Shadab, Surendra Adhikari, Anja Rutishauser, Cyril Grima, Marc Andre Hesse

Therefore, understanding the mechanism of ice layer formation is imperative for improved modeling of firn processes, surface mass balance, ice sheet evolution, and sea level projections.

In the literature the term ice layer has been used to refer to both permeable (MacFerrin et al., 2019; Machguth et al., 2016; Rennermalm et al., 2022) and impermeable layers (Ashmore et al., 2020; Brils et al., 2024; Culberg et al., 2021) with respect to meltwater percolation. Field studies have typically defined ice layers as visually transparent layers in firn cores and found their average density to be 843 ± 36 kg/m^3 (Harper et al., 2012b), 873 ± 25 kg/m^3 (Machguth et al., 2016), or 862 ± 38 kg/m^3 (Rennermalm et al., 2022). These densities are comparable to the pore close-off densities ranging from 752 to 871 kg/m^3 (Gregory et al., 2014) and may therefore be impermeable. However, at site A of the Dye-2 station used in this study such high densities are not reported (Samimi et al., 2020; Vandecrux et al., 2020) and the density permeability relationship for firn remains highly uncertain (Clerx et al., 2022). For the purpose of this study, we therefore use the term ice layer for a layer with a significant reduction in porosity that remains permeable unless mentioned otherwise.

As meltwater formed at the surface percolates into the underlying cold firn it refreezes and warms the firn by releasing latent heat of fusion (S. Colbeck, 1975, 1976). This allows a wetting front to propagate downward into the firn but it only leads to a small and uniform reduction in porosity. The formation of an ice layer therefore requires a mechanism that localizes refreezing in a narrow depth interval and leads to a larger porosity reduction. Field observations in snowpack show that ice layers can form when wetting front encounters a discontinuity, such as a stratigraphic horizon with reduced permeability. This leads to ponding of meltwater and the formation of a perched water table (Culberg et al., 2021; Marsh & Woo, 1984a, 1985; Miller et al., 2022). The conductive cooling of the ponded meltwater then causes refreezing, reduces the porosity, and leads to the formation of an ice layer along the discontinuity (Marsh & Woo, 1984a; Pfeffer & Humphrey, 1998). Current models of ice layer formation in firn therefore also assume that ponding on a pre-existing discontinuity localizes the freezing process (Humphrey et al., 2021; Pfeffer & Humphrey, 1998; Wever et al., 2016). While this process of ice layer formation undoubtedly occurs, primarily during rainfall onto snow pack, the ponding of meltwater on a pre-existing discontinuity requires either a large meltwater flux or a strong reduction in permeability (Brils et al., 2024; Pfeffer & Humphrey, 1998; M. Shadab & Hesse, 2022). Data from the Dye-2 station in southwest Greenland show that even an extreme melt event produces insufficient melt fluxes to lead to significant ponding on pre-existing discontinuities within the firn (Samimi et al., 2020; Vandecrux et al., 2020). Instead, melt is observed to penetrate past significant pre-existing discontinuities and refreeze at greater depth, forming a new ice layer

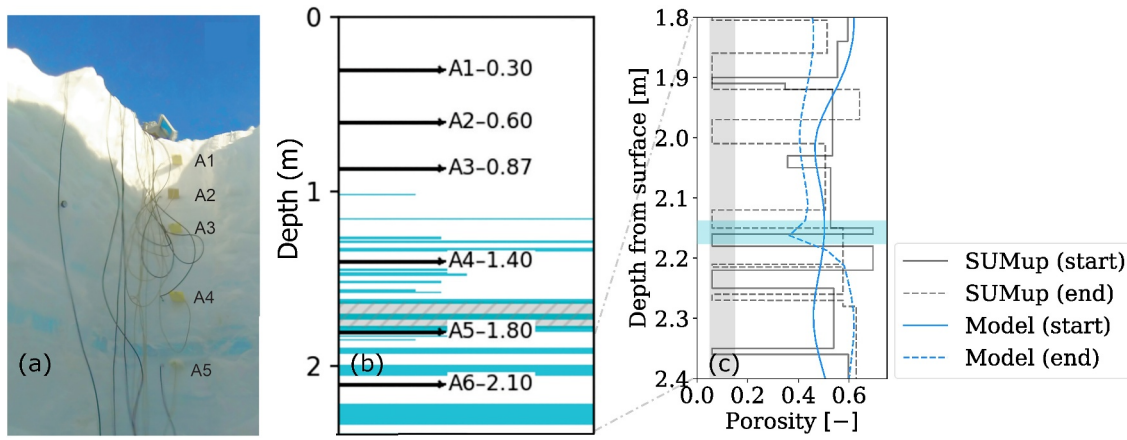

Figure 1. Ice layers in glacial firn at the field site Dye-2 (Site-A) in southwest Greenland during summer of 2016 (Samimi et al., 2020): (a) Photograph of the firn stratigraphy and TDR sensor distribution at the site. (b) Ice layer stratigraphy of Site-A shown in panel a. Blue colors show the location and thickness of ice layers, and black arrows indicate the depths (in m) of thermistors and Time Domain Reflectometer (TDR) probes. The gray hatched zone highlights an 11-cm-thick ice layer just above Level A5. (c) The initial and final porosity profiles before (start) and after (end) the summer 2016 melting season. Both field observations from the SUMup database (Montgomery et al., 2018; Rennermalm et al., 2022) and modeling results for this study are shown. The SUMup data at Dye-2 comes from a borehole other than site-A and at the beginning of 2016 summer melt season is referred to as start whereas the 2017 spring data, extracted after removing the winter snow facies, is referred to as end. The depth from surface is different from absolute depth (z) as the surface can ablate. The gray box is the region of open (pore close-off) porosity lying between 5% and 18% (Gregory et al., 2014; Rennermalm et al., 2022; Rutishauser et al., 2024). A new ice layer formed at about 2.15 m below the surface is corroborated by the field data (shown in blue box).

(Figure 1c). As such, it is currently not clear how ice layers form in firn where meltwater fluxes are too small to trigger the formation of perched water tables.

Here we propose a different mechanism based on the interplay of heat advection and conduction that localizes the refreezing and does not require pre-existing heterogeneities within the firn. The amount of refreezing due to heat advection can be quantified based on the energy balance between the latent heat of infiltrating meltwater and the cold content (sensible heat) of the firn (Clark et al., 2017). A simple heat conduction model suggests a necessary condition for refreezing is that it must occur at a much shorter timescale than the infiltration period (Pfeffer et al., 1991). Although past studies have explored some of these aspects of thermomechanics (Humphrey et al., 2021; Wever, et al., 2016), sufficient consideration of heat advection and conduction is lacking, especially at the large spatial scales where Darcy's law holds and in light of realistic thermal forcings at the firn surface. We present simulations with a multiphase thermomechanical model that unravel the mechanism and factors controlling ice layer formation and adequately predict the main features of ice layers measured at the Dye-2 station in southwest Greenland (Samimi et al., 2020; Vandecrux et al., 2020).

2. Model Description

The present work extends the variably-saturated flow framework developed by M. A. Shadab and Hesse (2024) to study cold firn by utilizing enthalpy formulation (Alexiades & Solomon, 2018; Aschwanden et al., 2012; Carnahan et al., 2022) and is similar to the firn model of Meyer and Hewitt (2017). The enthalpy formulation has the advantage that the phase transition does not have to be smeared over a temperature interval as in Clark et al. (2017) and does not require variable switching. Our continuum thermomechanical model considers the three-phase mixture of porous ice with liquid water (subscript w), and gas as the pore fluids. The model assumes no participation of gas in fluid mechanics and thermodynamics and no compaction of the firn. Section S1 in Supporting Information S1 describes the mathematical model, numerical framework, and validation with analytic solutions. The values of all thermodynamical and hydrological variables used in this model are summarized in Table S1 in Supporting Information S1.

3. Results

3.1. A Single Extreme Melting Event

To understand the relative impact of the modes of heat transfer at various stages of meltwater infiltration and refreezing, we first study simplified numerical experiments before considering simulations driven by complex field data. Initially, we study the evolution of a single 4-day melt infiltration event on a homogeneous dry and cold firn with an initial temperature of $T = -10°C$ and porosity of $\phi = 0.5$. This model problem is inspired by the melt event at the Dye-2 station during 9–12 August 2016 (Samimi et al., 2020). Even during this extreme melting event, the Liquid Water Content (LWC) at the surface of the snow remains very low at approximately 0.03. Here we simply supply melt to the top of the domain at an infiltration rate of $2.47 \cdot 10^{-7}$ m/s which corresponds to an LWC of 0.03. Rather than melting the firn at the surface this simple boundary condition is similar to rain at 0°C infiltrating the firn and the elevation of the firn surface does not change. The results of this simulation are shown in Figures 2a–2d.

First, we consider melt infiltration in the absence of heat conduction (Figures 2a and 2b). In this limit, the dynamics are solely governed by propagation of kinematic waves of LWC (S. Colbeck, 1976; Clark et al., 2017; Meyer & Hewitt, 2017; Singh et al., 1997). Initially, a gravity-driven wetting front (shock wave) propagates downward with constant speed (Figure 2b). Freezing occurs only at the wetting front, where sufficient melt refreezes so that the release of latent heat warms the firn to the melting point. Due to the large latent heat this requires only small amounts of freezing that result in a negligible reduction in porosity from 0.5 to approximately 0.47 (Figure 2a). This drop can be calculated theoretically using a simple energy balance of the enthalpy of refrozen ice with the heat required to warm the surrounding firn to 0°C (S. C. Colbeck, 1979; Clark et al., 2017; Meyer & Hewitt, 2017; M. Shadab et al., 2024). Once the melt supply ceases, a spreading wave (rarefaction) in LWC forms in the temperate firn and forms a region of declining LWC. We refer to the leading edge of this drying region as the drying front (Figure 2b). The drying front in unsaturated flow always propagates faster than the associated wetting front (Smith, 1983) and once it reaches the wetting front at the interaction depth, z_i, the LWC at the front drops and its propagation slows down rapidly (Clark et al., 2017; Singh et al., 1997). However, the amount of freezing occurring at the front is not affected, because it is solely determined by the heat needed to raise

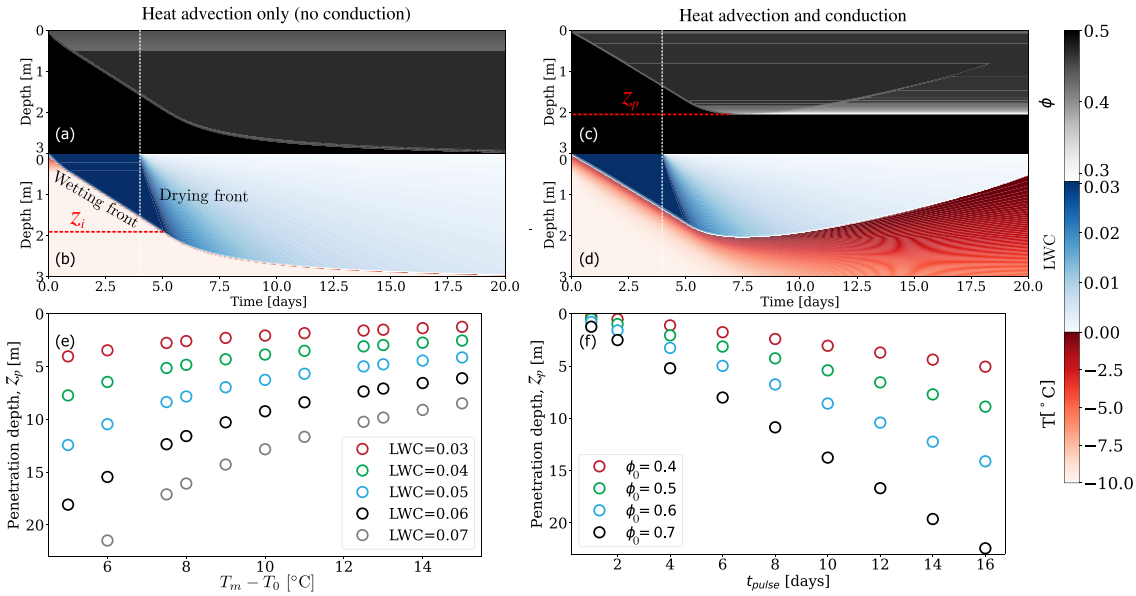

Figure 2. Dynamics of a single melt pulse infiltrating cold dry firn. In this example, we consider a single continuous melt event that lasts for 4 days (white dashed line) and the uniform firn column with initial liquid water content LWC = 0.03, temperature $T_0 = -10$°C, and porosity $\phi_0 = 0.5$. The evolution of (a) porosity and (b) LWC and temperature without the consideration of heat conduction. Panels (c) and (d) show the corresponding results that account for the effect of conduction. In (a), the wetting front can be seen propagating downward, leading to refreezing with a slight porosity reduction of 0.03. After 4 days, when the melt event ends, a drying front propagates downward with a much faster velocity. The fronts cross over at an interaction depth z_i (see b). The ice layer nucleates as soon as the waves start interacting, after which the infiltration rate reduces, leading to faster refreezing. The depth at which the ice layer forms is referred to as the penetration depth z_p (see c). Panels (e) and (f) show the dependence of penetration depth on the initial firn properties and the intensity (in terms of surface LWC) and duration (t_{pulse}) of the melt event. See corresponding Movies S1 and S2.

the firn temperature to the melting point. These results confirm that advective heat transport by meltwater percolation only leads to a small and uniform porosity reduction. Therefore, it does not lead to the formation of discrete ice layers in the firn. While the amount of porosity reduction can be modulated by changes in firn temperature or porosity with depth (S. Colbeck, 1975, 1976; Humphrey et al., 2021), neither leads to the strong localization of freezing required to form ice layers.

Next, we repeat this simulation with heat conduction as an additional heat transfer mechanism (Figures 2c and 2d). This leads to the formation of a conductive boundary layer ahead of the wetting front (Meyer & Hewitt, 2017). The width of the boundary layer is controlled by the dimensionless Péclet number *Pe* that describes the ratio of the conductive to advective time scales for heat transfer across the firn (Humphrey et al., 2021; Pfeffer et al., 1991). The thin boundary layer in Figure 2d demonstrates that the advection is dominant during meltwater infiltration (Pe $\gg$ 1). Neither the terminal speed of the wetting front nor the porosity reduction across the front are affected by conduction, because they are controlled solely by the mass and energy balance across the front (Logan, 2008). After the melt supply ceases, the drying front rapidly propagates into the firn. Once it reaches the wetting front at z_i melt percolation slows rapidly and conduction becomes the dominant heat transfer mechanism ($Pe \ll 1$). This is evident in the widening of the conductive boundary layer after the wetting and drying fronts have met (Figure 2d). This freezes the remaining meltwater almost in place and leads to a stark porosity reduction from 0.5 to 0.27 just below the depth where the fronts meet (Figure 2c). We refer to the depth of ice layer formation as the penetration depth, z_p. While it is possible to choose model parameters to completely eliminate the porosity, it is unlikely that a single melting event forms an impermeable ice layer under natural conditions.

We summarize the mechanism of ice layer formation as a three-stage process. First, a wetting front propagates downward during the meltwater supply. Next, the end of melt supply generates a drying front that propagates downward at a much faster speed. Finally, the interactions between the two fronts lead to a switch from an advection-dominated to a conduction-dominated thermal regime. This localizes the freezing and causes a sudden drop in porosity, which we call the ice layer. As such, the variation in melt supply and the switch in dominant heat transfer modes are the necessary conditions for ice layer formation. Both the mechanism proposed here and the ponding on pre-existing discontinuities induce ice layer formation by slowing the vertical meltwater percolation.

In our model the percolation slows because of the inherent non-linearity of unsaturated flow, where the relative permeability drops quickly once saturation at the front declines (Clark et al., 2017). In heterogeneous firn these two mechanisms will interact and enhance each other.

Our proposed mechanism is independent of the choice of firn properties and the volume and duration of meltwater supply, but the resulting ice structure is modulated by those properties. Figures 2e and 2f summarize the impact of initial firn properties and boundary forcing on the ice layer formation depth, z_p, in homogeneous firn. A higher initial firn temperature leads to a faster and deeper percolation due to less refreezing (Figure 2e). A larger meltwater supply (plotted in terms of the surface LWC in Figure 2e) increases penetration depth as the propagation speed of the wetting front increases proportionally, and conduction takes longer to dominate over advection after the fronts interact. Similarly, a longer melt supply t_{pulse} increases the penetration depth (Figure 2f). Finally, more porous firn holds a lesser cold (energy) content, sustains higher meltwater flux and therefore promotes deeper percolation.

We find that the depth of a newly formed ice layer is mainly controlled by the sensible heat of cold firn. Given the homogeneous firn properties and constant surface meltwater flux, we may estimate the depth of the ice layer following a single melt event as follows (see Section S2 in Supporting Information S1):

$$z_p = C\frac{I\,L}{(1-\phi_0)\,c_p\,(T_m - T_0)}t_{pulse}. \tag{1}$$

Here I is the volumetric meltwater flux, L is the latent heat of fusion of water, T_m is the melting temperature of ice, c_p is the specific heat of ice. Also, T_0 and ϕ_0 are the initial temperature and porosity of the homogeneous firn. The coefficient C is experimentally found to be a constant in the range of 0.6–0.8 (see Section S2 and Figure S2 in Supporting Information S1).

3.2. Successive Melting Events

The radiative surface heating and snow melting generally exhibit cyclic patterns. Classic examples include diurnal and seasonal variability. The net surface heat flux, Q_{net}, rather than the meltwater flux, I, is the primary field observable (Samimi et al., 2020), so we consider it a model forcing in the following experiments. To examine the meltwater percolation and ice layer formation processes in such conditions, we consider a sinusoidal heat flux described by $Q_{net}(t) = \overline{Q} + \Delta Q\sin(\omega t)$, where t is the time variable. The forcing frequency is $\omega = 2\pi/\mathcal{T}$, where $\mathcal{T}$ is the period of one cycle and $\overline{Q}$ is the mean heat flux.

For a heat flux with zero mean over complete periods $\left(\overline{Q} = 0\right)$, the condition for surface melting can be evaluated analytically (see Section S3 in Supporting Information S1). The regime diagram in Figure 3i highlights the main results showing the effect of cyclic heat flux on surface melting. The regime boundary corresponds to the dimensionless critical flux varying linearly with the dimensionless temperature deficit. The critical heat flux amplitude ΔQ_c required to cause melting increases with the temperature difference $(T_m - T_0)$ as more heat is needed to warm the firn. Increasing the forcing frequency ω decreases the skin depth $\sqrt{\overline{\alpha}/\omega}$ and, hence, increases the heat flux required for melting. The effect of porosity ϕ is embedded in the thermodynamic properties of cold firn, namely, effective thermal conductivity $\overline{\kappa} \propto (1-\phi)^l$ and thermal diffusivity $\overline{\alpha}$, defined as $\overline{\kappa}/\overline{\rho c_p}$ with $\overline{\rho c_p} \equiv \rho c_p(1-\phi)$ and ρ being the density of ice and c_p being thermal conductivity of ice. Therefore, the critical heat flux decreases with increasing porosity as $\Delta Q_c \propto (1-\phi)^{(l-1)/2}$ with $l = 1.885$ (Yen, 1981). In summary, melting is more readily caused by high amplitude and low-frequency heat flux on a more porous firn.

First, we consider a case of zero mean heat flux, $\overline{Q} = 0$ (Figures 3a–3d). Meltwater is produced when $\Delta Q > \Delta Q_c$ during the warm phase ($Q_{net} > 0$) which lowers the firn surface (Figure 3i). This melt percolates downward into the firn where it forms an ice layer with reduced porosity during the subsequent cold phase, similar to the previous case. In the cold phase that follows ($Q_{net} < 0$), the near-surface firn temperature drops from its initial value of -10°C to about -20°C (Figure 3c). In each subsequent cycle, less melt is generated as the critical flux amplitude ΔQ_c increases due to a porosity reduction and a larger temperature deficit in the firn near the surface (Figure 3i). The reduced meltwater has to overcome colder and denser firn, partly due to previously-formed ice layers, leading to a shallower penetration depth after each cycle (Figure 3d). The shallow ice layers form from the bottom up,

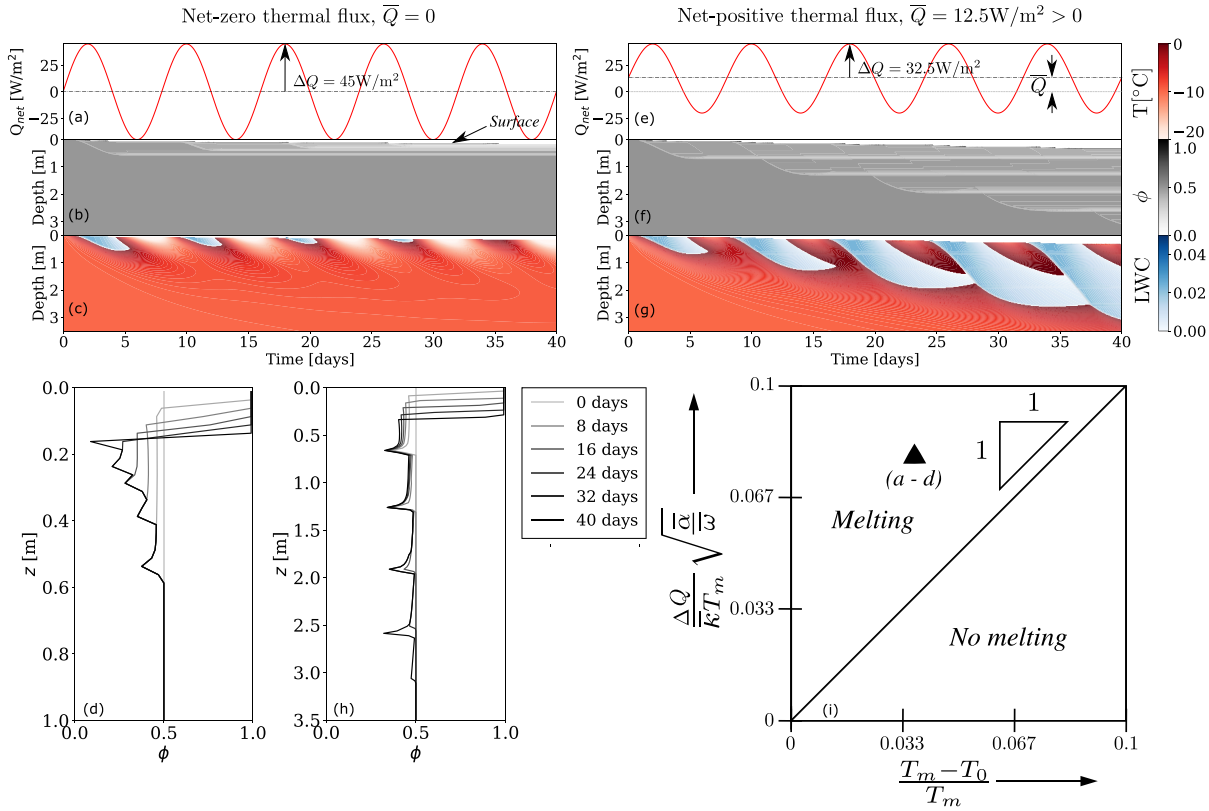

Figure 3. Dynamics of meltwater percolation following cyclic melt events. The initial firn properties are the same as in the previous experiment. Five sinusoidal cycles of net heat flux Q_{net} with a periodicity of $\mathcal{T} = 8$ days are applied at the surface. The simulation runs for five complete heat flux cycles until 40 days have passed. We consider the two cases of (a) net-zero and (e) net-positive heat flux, with zero and positive mean during the cyclic forcing, respectively. The corresponding evolution of porosity and temperature (red) along with liquid water content (blue) and resulting porosity profiles respectively are shown in panels (b) to (d) for net-zero and (f) to (h) for net-positive heat flux forcings. In the first case, less porous ice layers form near the surface, while more porous deeper layers form in the case of net-positive forcing. (i) A regime diagram showing the melt condition for a cyclic thermal forcing with $\overline{Q} = 0$ using temperature in kelvins. The data point indicated with a triangle corresponds to the net-zero forcing that leads to melt generation, as shown in panels (a)–(d). See Supporting Information S1 (Section S3, Movies S3 and S4 and Figures S3–S5) for more results. The completely melted firn above the firn surface is removed, shown in white, in this paper.

with increasingly reduced porosity. Despite a significant reduction in porosity, the meltwater never ponds on top of the ice layer to form a perched aquifer and the mechanism remains the same.

Next, we explore a warming trend with a positive mean heat, $\overline{Q} > 0$, similar to the conditions at the Dye-2 site (Figures 3e–3h). In this case, the near-surface firn warms gradually with each successive cycle, which leads to more melting and deeper meltwater percolation (Figures 3f and 3g). The residence time of meltwater increases with each melt cycle because the firn remains warmer during the cold phases, allowing meltwater to percolate past the pre-existing ice layers. Ice layer formation therefore happens at increasingly greater depths where the meltwater encounters cold firn (Figure 3h). In Figures S4 and S5 in Supporting Information S1 we show that $\overline{Q}$ must exceed a small positive threshold $\overline{Q}_c$ for the formation of deep ice layers.

These idealized experiments show that small changes in the surface thermal forcing can lead to radically different patterns of ice layers within the firn. Despite their simplicity our results hint at the possibility that the background climatic regime can be recorded in the pattern of ice layers. In a cold climate with subcritical mean heat flux, $\overline{Q} < \overline{Q}_c$, ice layers are formed from the bottom up in a tight sequence near the surface with increasingly lower porosity (Figure 3d). In subsequent melt events perched aquifers may form on these ice layers and lead to lateral meltwater routing. Conversely, in a warming thermal regime, $\overline{Q} > \overline{Q}_c$, the depth distribution of ice layers is wider and deeper. These layers maintain more porosity than those formed in cold climate and form in a top-down sequence (Figure 3h). In this case, the capacity of the firn to store meltwater is greater and the formation of perched aquifers is less likely. The critical mean flux, $\overline{Q}_c$, indicative of the switch from a top-down to a bottom-up

ice layer formation regime, may depend on climate forcing (amplitude and time period of surface heat flux), firn properties (thermal diffusivity, temperature, porosity) and fluid infiltration variables (meltwater flux, absolute and relative permeabilities). For the idealized model studied here, based on melt events at the Dye-2 station, the critical mean heat flux $\overline{Q}_c$ is around 2.5 W/m^2 (Figures S4 and S5 in Supporting Information S1).

In both climatic conditions, increasing the periodicity, $\mathcal{T}$, of the heat flux leads to deeper ice layers (Figure S3 in Supporting Information S1). Given a heat flux time series and firn properties, these results may help predict whether ice layers form near the surface or deeper into the firn. It may also be possible to deduce past climatic regimes and the intensity and frequency of extreme melt events from ice layers detected by radar stratigraphy or retrieved by firn coring.

4. Meltwater Percolation and Refreezing at Dye-2 in Southwest Greenland

Lastly, we model a real-world scenario based on the field data from the Dye-2 station in the summer of 2016 (Samimi et al., 2020; Vandecrux et al., 2020) and interpret the results in light of the understanding derived from the idealized experiments considered above. We initialize the firn properties, including the depth-varying porosity and temperature, with the field data (see Section S1.4 in Supporting Information S1). We allow the firn surface elevation to evolve and apply the boundary conditions for heat flux and snow accumulation constrained by the field measurements (Figure 4a). This site contains a significant pre-existing ice layer at a depth between 1.2 and 1.5 m depth. It is therefore a good site to test if ice layer is formed by meltwater perching on this pre-existing discontinuity or by the mechanism proposed here.

The time series of heat flux Q_{net} shows two extreme melt events on 18–20 July and 9–12 August 2016. The flux forcing is analogous to the net-positive scenario (Figure 3e), in which the firn gradually warms over time and meltwater percolates increasingly deeper into the firn (Figure 4c). A sustained positive heat flux of lesser magnitude ($\sim$10 W/m^2) was measured between the two extreme events and generated an almost continuous melt supply (Figure 4a). During this time the speed of the wetting front slows down due to reduced melt supply and the interaction with a pre-existing ice layer. After the surface melting ceases this meltwater refreezes within the pre-existing ice layer and reduces its porosity.

The second meltwater pulse generated during the extreme melting event in August penetrates deeper because the firn above the ice layer has been warmed by previous melting events (Figures 4c and 4e). The meltwater from this event percolates past the pre-existing ice layer and refreezes to form a new ice layer at approximately 2.4 m depth by the mechanism proposed here (Figures 4b and 4c). Ponding and formation of a perched aquifer in the pre-existing ice-layer at Dye-2 requires a meltwater flux exceeding 10^{-4} m/s (M. Shadab & Hesse, 2022), but even this extreme melt event produces a flux of only $\sim 10^{-7}$ m/s (Figure S6 in Supporting Information S1). As such, the interaction with the ice layer only locally doubles the LWC to 0.06. The depth of the newly formed ice layer in our model matches the meltwater penetration depth of 2.4 m determined from upward-looking ground-penetrating radar (upGPR) during the extreme melting event from 9 to 12 August 2016 (Figure 4c). No direct observations of changes in firn stratigraphy due to these melting events are available for Site-A at the Dye-2 station. However, the SUMup database (Montgomery et al., 2018; Rennermalm et al., 2022) for a different site at the Dye-2 station does show the formation of a new ice layer at about 2.15 m depth below the surface (Figure 1c, Figure S12 in Supporting Information S1). While the lateral heterogeneity makes it difficult to correlate ice layers even between neighboring sites, this observation does provide supporting evidence for the ice layer formation mechanism proposed here. There is a discrepancy of about 0.2 m in surface ablation measured between upGPR and our model that transcends to an uncertainty of about 0.2 m in the ice layer depth when compared against SUMup data. This uncertainty in surface location stems from errors in the measurement and model implementation of the surface thermal flux and accumulation boundary conditions.

5. Discussion

Ice layer formation requires the localization of the refreezing within the firn. The standard mechanism requires the ponding of melt on a pre-existing discontinuity, but we have argued that melt fluxes are too small for ponding. Instead we have proposed a different localization mechanism that occurs naturally after a melting cycle as the drying front catches up with the wetting front. Our mechanism can explain the observations from the Dye-2 site

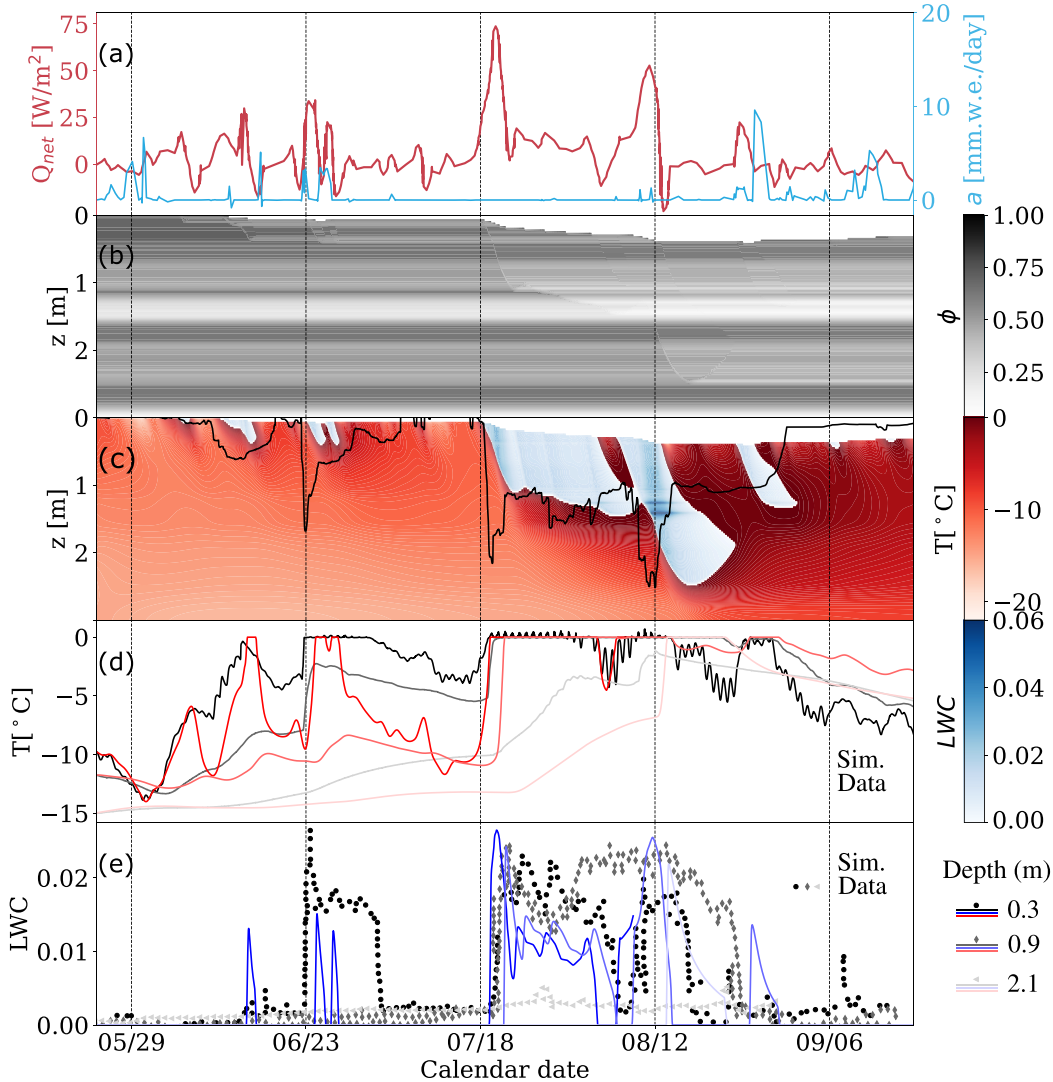

Figure 4. Meltwater percolation and ice layer formation at the Site A of Dye-2 Station in southwestern Greenland during the summer of 2016. (a) Measured heat flux Q_{net} and surface accumulation rate a (Samimi et al., 2020; Vandecrux et al., 2020). (b) Modeled porosity ϕ showing surface erosion and ice layers (whiter bands). (c) Modeled liquid water content LWC (blue) and temperature T evolution (red). The black line shows the water percolation depth measured by the upward-looking ground penetrating radar (upGPR) (Heilig et al., 2018). (d) Temperature evolution at specific depths from model simulations (red) and thermistor measurements (Samimi et al., 2020) (black). (e) The resulting LWC from simulations (blue) and measurements (black). The "measured" LWC is derived from a dielectric mixing model and subjected to uncertainty (Samimi & Marshall, 2017; Samimi et al., 2020). Movie S5 and Figure S6 in Supporting Information S1 correspond to this figure.

where the melt generated by an extreme melt event percolated past a pre-existing ice layer (Figure 4b) and forms a new ice layer at greater depth (Figure 1c).

This conclusion requires that the pre-existing ice layer is permeable. For consistency with previous simulations of the Dye-2 site, our initial firn porosity profile is based on the same firn density measurements used in the RetMIP study (Vandecrux et al., 2020). These density measurements average the firn properties over 10 cm intervals and it is possible that a thin, high density, impermeable ice layer is smeared into a thicker, lower density, permeable ice layer. In this case, melt should pond on the impermeable ice layer and refreeze according to the standard ice layer formation model. Taken the measured initial ice-layer density of 715 kg/m^3 at face value, the porosity of 0.22 would exceed the pore close-off and allow melt percolation. It is possible that the averaging in the measurements

obscures that the ice-layer is thinner, denser and lower porosity. To test this we have derived conditions required for ponding in Section S4 in Supporting Information S1. Our results show that the density of the pre-existing ice layer would have to exceed 798 kg/m^3 ($\phi \leq 0.13$) for ponding to occur, given the observed melt fluxes and firn temperatures. While we cannot exclude this possibility, we argue that the simplest interpretation of the observations at the Dye-2 station, that is, melt percolated past the pre-existing ice layer and formation of a new ice layer at greater depth, is that the pre-existing ice layer was permeable.

Past attempts at modeling data from the Dye-2 site have focused on matching the observed melt percolation depth and showed large discrepancies between different models (Vandecrux et al., 2020). Predicted percolation depths for the second melt event range between 1.4 and 10.2 m (Table S2 in Supporting Information S1). Our model uses the same physical parameters as those reported by other Darcy-based models, for example, Meyer and Hewitt (2017), and they are summarized in Table S1 in Supporting Information S1. The larger penetration depth in our simulations relative to Meyer and Hewitt (2017) is likely due to the use of an experimentally determined non-linear relation for the effective thermal conductivity of firn (Yen, 1981). This predicts lower near-surface firn conductivities which leads to more rapid warming of the surface and increases overall melt production. Also, we do not use an irreducible water saturation (S. Colbeck, 1976; Coléou & Lesaffre, 1998), because meltwater infiltration into firn is an imbibition process (Blunt, 2017). This increases the speed of the wetting front and hence the penetration depth (Figure S7 in Supporting Information S1). Finally, we note that the ice-layer formation process proposed here should be observed in any firn hydrology model that considers both unsaturated Darcy flow, heat conduction and phase change. The reason this has not been previously noticed in similar models is likely either that the study focused on other aspects of firn hydrology (Vandecrux et al., 2020), the set up did not lead to the interaction of wetting and drying fronts (Meyer & Hewitt, 2017) or they may have been obscured by other model complexities (Moure et al., 2023).

However, our model has difficulty matching the speed of the wetting front and earlier isolated melting events. The mismatch in the speed of the wetting front cannot be improved simply by increasing the firn permeability because this also increases the penetration depth. Instead we suggest that this may either be due to the lack of local thermal equilibrium between the melt and the ice (Rees et al., 2008) or due to preferential flow (Nimmo, 2012, 2021). A fluid out of thermal equilibrium can penetrate faster into the firn, because less mass is lost due to solidification initially (Moure et al., 2023). This could also explain why thermistors record sub-zero temperatures below 1.8 m depth (shown at 2.1 m depth in Figure 4d) although upGPR detects percolation depth down to 2.4 m (Figure 4c). The lack of thermal equilibrium may also explain why isolated melting events in June penetrate deeper than our model suggests. An analysis of the effect of thermal disequilibrium on our proposed ice layer formation mechanism is an interesting direction of further work.

Preferential flow refers to the localization of the flow along preferred pathways and provides a mechanism for melt to penetrate deeper into the firn by preventing thermal equilibration with the bulk of the firn (S. C. Colbeck, 1979; Marsh & Woo, 1984b). It has been observed both in laboratory experiments (Katsushima et al., 2013) and in the field in the form of near-vertical ice pipes in firn (Humphrey et al., 2012). In the one-dimensional models commonly used in firn hydrology (Stevens et al., 2020), preferential flow is represented using a dual-domain approach (Wever et al., 2016). Multi-dimensional models for gravitational preferential flow have also been presented (Hirashima et al., 2014; Leroux et al., 2020; Moure et al., 2023) but are challenging to compare with one-dimensional field data. At the Dye-2 site the community firn model that uses dual-domain approach for preferential flow significantly over-predicts the penetration depth (Vandecrux et al., 2020) (Table S2 in Supporting Information S1).

On the other hand, the ability of our one-dimensional model to match the penetration depth without parameter tuning may suggest that the meltwater percolation was relatively uniform during the second melting event. The lack of preferential flow could be due to the very low water fluxes during these melt events, $|\mathbf{q}| \sim 10^{-7}$ m/s (Figure S6 in Supporting Information S1). Experimental work on infiltration in sands, shows that preferential flow is suppressed for $|\mathbf{q}| \ll 10^{-1}$ m/s (DiCarlo, 2013; Yao & Hendrickx, 1996). It is worth noting that dye tracer experiments in the field that are used to visualize preferential flow, both in soil and snow/firn, are conducted at meltwater fluxes that are likely orders of magnitudes higher than those produced by melting. As such, the determination of the conditions when melting in firn leads to preferential flow is another interesting direction of future investigation.

6. Conclusion

This study presents a mechanism for the formation of ice layers in firn that does not require the perching of meltwater on pre-existing discontinuities. A different mechanism is required because even extreme melting events produce insufficient meltwater fluxes to cause perching on any but the least permeable ice layers. Instead, we show that refreezing of meltwater naturally localizes after the end of surface melting, when the drying front catches up to the wetting front. This causes a rapid drop in saturation and arrests the wetting front. The switch from advective to conductive heat transfer then freezes the remaining melt at the almost stationary wetting front to form an ice layer. Our model can explain and reproduce the percolation of meltwater past a pre-existing ice layer at the Dye-2 site and the formation of a new ice layer at greater depth.

Because our mechanism is independent of pre-existing firn structure it is responsive to the thermal environment of the firn. In particular, our model suggests that the sequencing of subsequent ice layers is sensitive to overall heat budget. Warming conditions, allow the meltwater to penetrate increasingly deeper into the firn, enhancing the meltwater storage in the firn and preventing the formation of impermeable ice layers that lead to lateral meltwater routing. In contrast, subsequent melting events tend to reinforce shallow ice layers if the heat budget of the firn is constant. Our results suggest the possibility that the arrangement and character of ice layers in firn contains information about past climatic trends.

Data Availability Statement

All the data needed to evaluate the conclusions of the article are present in the manuscript and the files in Supporting Information S1. All codes used for numerical simulations are available on Zenodo (M. A. Shadab et al., 2024) linked to GitHub repository: https://github.com/mashadab/ice-layer-formation for reproducibility. It contains scripts to produce Figures 2–4. The field data from Vandecrux et al. (2020); Samimi et al. (2021) is re-uploaded to the GitHub repository to run the code corresponding to Figure 4.

Acknowledgments

M.A.S. acknowledges the financial support received through the University of Texas Institute for Geophysics (UTIG) Blue Sky Student Fellowship and NASA Jet Propulsion Laboratory Graduate Fellowship. Acknowledgment is made to the donors of the American Chemical Society Petroleum Research Fund for partial support of this research. This research project was also supported by NASA-EW Grant 80NSSC19K0505 to M. A.H. Part of this research was carried out at the Jet Propulsion Laboratory, California Institute of Technology, under a contract with the National Aeronautics and Space Administration (Grant 21-ESI21-0011 awarded to S.A.). A.R. has been supported by the Greenland Climate Network (GC-Net) monitoring program. The authors would like to thank Achim Heilig for sharing and discussing the upward-facing ground-penetrating radar data, and also Shawn Marshall and Andreas Colliander for providing the Dye-2 data. Furthermore, insightful discussions with Xiaojing Fu and Christopher Max Stevens are greatly acknowledged. The authors also thank Colin Meyer and one anonymous reviewer for their helpful comments that improved the quality of the manuscript.

References

Alexiades, V., & Solomon, A. D. (2018). *Mathematical modeling of melting and freezing processes*. Routledge.

Alley, K., Scambos, T., Miller, J., Long, D., & MacFerrin, M. (2018). Quantifying vulnerability of Antarctic ice shelves to hydrofracture using microwave scattering properties. *Remote Sensing of Environment*, *210*, 297–306. https://doi.org/10.1016/j.rse.2018.03.025

Aschwanden, A., Bueler, E., Khroulev, C., & Blatter, H. (2012). An enthalpy formulation for glaciers and ice sheets. *Journal of Glaciology*, *58*(209), 441–457. https://doi.org/10.3189/2012jog11j088

Ashmore, D. W., Mair, D. W. F., & Burgess, D. O. (2020). Meltwater percolation, impermeable layer formation and runoff buffering on Devon Ice Cap, Canada. *Journal of Glaciology*, *66*(255), 61–73. https://doi.org/10.1017/jog.2019.80

Bell, R. E., Banwell, A. F., Trusel, L. D., & Kingslake, J. (2018). Antarctic surface hydrology and impacts on ice-sheet mass balance. *Nature Climate Change*, *8*(12), 1044–1052. https://doi.org/10.1038/s41558-018-0326-3

Blunt, M. (2017). *Multiphase flow in permeable media*. Cambridge University Press. https://doi.org/10.1017/9781316145098

Brils, M., Munneke, P. K., Jullien, N., Tedstone, A. J., Machguth, H., van de Berg, W., & van den Broeke, M. (2024). Climatic drivers of ice slabs and firn aquifers in Greenland. *Geophysical Research Letters*, *51*(3), e2023GL106613. https://doi.org/10.1029/2023gl106613

Carnahan, E., Vance, S., Cox, R., & Hesse, M. (2022). Surface-to-ocean exchange by the sinking of impact generated melt chambers on Europa. *Geophysical Research Letters*, *49*(24), 1–12. https://doi.org/10.1029/2022GL100287

Chan, K., Grima, C., Rutishauser, A., Young, D. A., Culberg, R., & Blankenship, D. D. (2022). Spatial characterization of near-surface structure and meltwater runoff conditions across Devon ice cap from dual-frequency radar reflectivity. In *The cryosphere discussions* (pp. 1–22).

Clark, M. P., Nijssen, B., & Luce, C. H. (2017). An analytical test case for snow models. *Water Resources Research*, *53*(1), 909–922. https://doi.org/10.1002/2016wr019672

Clerx, N., Machguth, H., Tedstone, A., Jullien, N., Wever, N., Weingartner, R., & Roessler, O. (2022). In situ measurements of meltwater flow through snow and firn in the accumulation zone of the SW Greenland ice sheet. *The Cryosphere*, *16*(10), 4379–4401. https://doi.org/10.5194/tc-16-4379-2022

Colbeck, S. (1975). *An anlysis of hydrologic response to rain-on-snow (Tech. Rep.)* (p. 340). Cold Regions Research and Engineering Laboratory.

Colbeck, S. (1976). An analysis of water flow in dry snow. *Water Resources Research*, *12*(3), 523–527. https://doi.org/10.1029/WR012i003p00523

Colbeck, S. C. (1979). Water flow through heterogeneous snow. *Cold Regions Science and Technology*, *1*(1), 37–45. https://doi.org/10.1016/0165-232x(79)90017-x

Coléou, C., & Lesaffre, B. (1998). Irreducible water saturation in snow: Experimental results in a cold laboratory. *Annals of Glaciology*, *26*, 64–68. https://doi.org/10.1017/s0260305500014579

Culberg, R., Schroeder, D. M., & Chu, W. (2021). Extreme melt season ice layers reduce firn permeability across Greenland. *Nature Communications*, *12*(1), 2336. https://doi.org/10.1038/s41467-021-22656-5

de la Peña, S., Howat, I. M., Nienow, P. W., van den Broeke, M. R., Mosley-Thompson, E., Price, S. F., et al. (2015). Changes in the firn structure of the western Greenland Ice Sheet caused by recent warming. *The Cryosphere*, *9*(3), 1203–1211. https://doi.org/10.5194/tc-9-1203-2015

DiCarlo, D. (2013). Stability of gravity-driven multiphase flow in porous media: 40 Years of advancements. *Water Resources Research*, *49*(8), 4531–4544. https://doi.org/10.1002/wrcr.20359

Gascon, G., Sharp, M., Burgess, D., Bezeau, P., & Bush, A. B. G. (2013). Changes in accumulation-area firn stratigraphy and meltwater flow during a period of climate warming: Devon Ice Cap, Nunavut, Canada. *Journal of Geophysical Research: Earth Surface*, *118*(4), 2380–2391. https://doi.org/10.1002/2013JF002838

Gregory, S., Albert, M., & Baker, I. (2014). Impact of physical properties and accumulation rate on pore close-off in layered firn. *The Cryosphere*, *8*(1), 91–105. https://doi.org/10.5194/tc-8-91-2014

Harper, J., Humphrey, N., Pfeffer, W. T., Brown, J., & Fettweis, X. (2012a). Greenland ice-sheet contribution to sea-level rise buffered by meltwater storage in firn. *Nature*, *491*(7423), 240–243. https://doi.org/10.1038/nature11566

Harper, J., Humphrey, N., Pfeffer, W. T., Brown, J., & Fettweis, X. (2012b). Greenland ice-sheet contribution to sea-level rise buffered by meltwater storage in firn. *Nature*, *491*(7423), 240–243. https://doi.org/10.1038/nature11566

Heilig, A., Eisen, O., MacFerrin, M., Tedesco, M., & Fettweis, X. (2018). Seasonal monitoring of melt and accumulation within the deep percolation zone of the Greenland ice sheet and comparison with simulations of regional climate modeling. *The Cryosphere*, *12*(6), 1851–1866. https://doi.org/10.5194/tc-12-1851-2018

Hirashima, H., Yamaguchi, S., & Katsushima, T. (2014). A multi-dimensional water transport model to reproduce preferential flow in the snowpack. *Cold Regions Science and Technology*, *108*, 80–90. https://doi.org/10.1016/j.coldregions.2014.09.004

Horlings, A. N., Christianson, K., & Miège, C. (2022). Expansion of firn aquifers in southeast Greenland. *Journal of Geophysical Research: Earth Surface*, *127*(10), e2022JF006753. https://doi.org/10.1029/2022jf006753

Humphrey, N. F., Harper, J. T., & Meierbachtol, T. W. (2021). Physical limits to meltwater penetration in firn. *Journal of Glaciology*, *67*(265), 952–960. https://doi.org/10.1017/jog.2021.44

Humphrey, N. F., Harper, J. T., & Pfeffer, W. T. (2012). Thermal tracking of meltwater retention in Greenland's accumulation area. *Journal of Geophysical Research*, *117*(F1), F01010. https://doi.org/10.1029/2011jf002083

Jiahong, W., Jiancheng, K., Jiankang, H., Zichu, X., Leibao, L., & Dali, W. (1998). Glaciological studies on the king George Island ice cap, South Shetland Islands, Antarctica. *Annals of Glaciology*, *27*, 105–109. https://doi.org/10.3189/1998aog27-1-105-109

Jullien, N., Tedstone, A. J., Machguth, H., Karlsson, N. B., & Helm, V. (2023). Greenland ice sheet ice slab expansion and thickening. *Geophysical Research Letters*, *50*(10), e2022GL100911. https://doi.org/10.1029/2022GL100911

Kaczmarska, M., Isaksson, E., Karlöf, L., Brandt, O., Winther, J.-G., Van De Wal, R. S., et al. (2006). Ice core melt features in relation to Antarctic coastal climate. *Antarctic Science*, *18*(2), 271–278. https://doi.org/10.1017/s0954102006000319

Katsushima, T., Yamaguchi, S., Kumakura, T., & Sato, A. (2013). Experimental analysis of preferential flow in dry snowpack. *Cold Regions Science and Technology*, *85*, 206–216. https://doi.org/10.1016/j.coldregions.2012.09.012

Leroux, N. R., Marsh, C. B., & Pomeroy, J. W. (2020). Simulation of preferential flow in snow with a 2-D non-equilibrium Richards model and evaluation against laboratory data. *Water Resources Research*, *56*(9), e2020WR027466. https://doi.org/10.1029/2020wr027466

Logan, J. (2008). *An introduction to nonlinear partial differential equations* (2nd ed.). John Wiley & Sons, Ltd.

MacFerrin, M., Machguth, H., As, D. v., Charalampidis, C., Stevens, C., Heilig, A., et al. (2019). Rapid expansion of Greenland's low-permeability ice slabs. *Nature*, *573*(7774), 403–407. https://doi.org/10.1038/s41586-019-1550-3

Machguth, H., Macferrin, M., Van As, D., Box, J. E., Charalampidis, C., Colgan, W., et al. (2016). Greenland meltwater storage in firn limited by near-surface ice formation. *Nature Climate Change*, *6*(4), 390–393. https://doi.org/10.1038/nclimate2899

Marsh, P., & Woo, M. (1984a). Wetting front advance and freezing of meltwater within a snow cover: 1. Observations in the Canadian Arctic. *Water Resources Research*, *20*(12), 1853–1864. https://doi.org/10.1029/WR020i012p01853

Marsh, P., & Woo, M. (1985). Meltwater movement in natural heterogeneous snow covers. *Water Resources Research*, *21*(11), 1710–1716. https://doi.org/10.1029/WR021i011p01710

Marsh, P., & Woo, M.-K. (1984b). Wetting front advance and freezing of meltwater within a snow cover: 1. Observations in the Canadian arctic. *Water Resources Research*, *20*(12), 1853–1864. https://doi.org/10.1029/wr020i012p01853

Meyer, C. R., & Hewitt, I. J. (2017). A continuum model for meltwater flow through compacting snow. *The Cryosphere*, *11*(6), 2799–2813. https://doi.org/10.5194/tc-11-2799-2017

Miller, J. Z., Culberg, R., Long, D. G., Shuman, C. A., Schroeder, D. M., & Brodzik, M. J. (2022). An empirical algorithm to map perennial firn aquifers and ice slabs within the Greenland ice sheet using satellite l-band microwave radiometry. *The Cryosphere*, *16*(1), 103–125. https://doi.org/10.5194/tc-16-103-2022

Montgomery, L., Koenig, L., & Alexander, P. (2018). The SUMup dataset: Compiled measurements of surface mass balance components over ice sheets and sea ice with analysis over Greenland. *Earth System Science Data*, *10*(4), 1959–1985. https://doi.org/10.5194/essd-10-1959-2018

Mouginot, J., Rignot, E., Bjørk, A. A., Van den Broeke, M., Millan, R., Morlighem, M., et al. (2019). Forty-six years of Greenland ice sheet mass balance from 1972 to 2018. *Proceedings of the National Academy of Sciences of the United States of America*, *116*(19), 9239–9244. https://doi.org/10.1073/pnas.1904242116

Moure, A., Jones, N., Pawlak, J., Meyer, C., & Fu, X. (2023). A thermodynamic nonequilibrium model for preferential infiltration and refreezing of melt in snow. *Water Resources Research*, *59*(5), e2022WR034035. https://doi.org/10.1029/2022wr034035

Nimmo, J. R. (2012). Preferential flow occurs in unsaturated conditions. *Hydrological Processes*, *26*(5), 786–789. https://doi.org/10.1002/hyp.8380

Nimmo, J. R. (2021). The processes of preferential flow in the unsaturated zone. *Soil Science Society of America Journal*, *85*(1), 1–27. https://doi.org/10.1002/saj2.20143

Noël, B., Van De Berg, W. J., Lhermitte, S., Wouters, B., Machguth, H., Howat, I., et al. (2017). A tipping point in refreezing accelerates mass loss of Greenland's glaciers and ice caps. *Nature Communications*, *8*(1), 1–8. https://doi.org/10.1038/ncomms14730

Pfeffer, W. T., & Humphrey, N. F. (1998). Formation of ice layers by infiltration and refreezing of meltwater. *Annals of Glaciology*, *26*, 83–91. https://doi.org/10.3189/1998AoG26-1-83-91

Pfeffer, W. T., Meier, M. F., & Illangasekare, T. H. (1991). Retention of Greenland runoff by refreezing: Implications for projected future sea level change. *Journal of Geophysical Research*, *96*(C12), 22117–22124. https://doi.org/10.1029/91jc02502

Rees, D. A. S., Bassom, A. P., & Siddheshwar, P. G. (2008). Local thermal non-equilibrium effects arising from the injection of a hot fluid into a porous medium. *Journal of Fluid Mechanics*, *594*, 379–398. https://doi.org/10.1017/s0022112007008890

Rennermalm, Å. K., Hock, R., Covi, F., Xiao, J., Corti, G., Kingslake, J., et al. (2022). Shallow firn cores 1989–2019 in southwest Greenland's percolation zone reveal decreasing density and ice layer thickness after 2012. *Journal of Glaciology*, *68*(269), 431–442. https://doi.org/10.1017/jog.2021.102

Rutishauser, A., Grima, C., Sharp, M., Blankenship, D. D., Young, D. A., Cawkwell, F., & Dowdeswell, J. A. (2016). Characterizing near-surface firn using the scattered signal component of the glacier surface return from airborne radio-echo sounding. *Geophysical Research Letters*, *43*(24), 12–502. https://doi.org/10.1002/2016gl071230

Rutishauser, A., Scanlan, K. M., Vandecrux, B., Karlsson, N. B., Jullien, N., Ahlstrøm, A. P., et al. (2024). Mapping the vertical heterogeneity of Greenland's firn from 2011–2019 using airborne radar and laser altimetry. *The Cryosphere*, *18*(5), 2455–2472. https://doi.org/10.5194/tc-18-2455-2024

Samimi, S., & Marshall, S. J. (2017). Diurnal cycles of meltwater percolation, refreezing, and drainage in the supraglacial snowpack of Haig Glacier, Canadian Rocky Mountains. *Frontiers in Earth Science*, *6*. https://doi.org/10.3389/feart.2017.00006

Samimi, S., Marshall, S. J., & MacFerrin, M. (2020). Meltwater penetration through temperate ice layers in the percolation zone at dye-2, Greenland ice sheet. *Geophysical Research Letters*, *47*(15), e2020GL089211. https://doi.org/10.1029/2020gl089211

Samimi, S., Marshall, S. J., Vandecrux, B., & MacFerrin, M. (2021). Time-domain reflectometry measurements and modeling of firn meltwater infiltration at dye-2, Greenland. *Journal of Geophysical Research: Earth Surface*, *126*(10), e2021JF006295. https://doi.org/10.1029/2021jf006295

Shadab, M., & Hesse, M. (2022). Analysis of gravity-driven infiltration with the development of a saturated region. *Water Resources Research*, *58*(11), e2022WR032963. https://doi.org/10.1029/2022WR032963

Shadab, M., Rutishauser, A., Grima, C., & Hesse, M. A. (2024). A unified kinematic wave theory for melt infiltration into firn. *arXiv*, *2403*, 15996. https://arxiv.org/abs/2403.15996

Shadab, M. A., Adhikari, S., Rutishauser, A., Grima, C., & Hesse, M. A. (2024). mashadab/ice-layer-formation: v1.0.0. *Zenodo*. https://doi.org/10.5281/zenodo.12706191

Shadab, M. A., & Hesse, M. A. (2024). A hyperbolic-elliptic PDE model and conservative numerical method for gravity-dominated variably-saturated groundwater flow. *Advances in Water Resources*, *190*, 104736. https://doi.org/10.1016/j.advwatres.2024.104736

Singh, V., Bengtsson, L., & Westerstrom, G. (1997). Kinematic wave modelling of vertical movement of snowmelt water through a snowpack. *Hydrological Processes*, *11*(2), 149–167. https://doi.org/10.1002/(SICI)1099-1085(199702)11:2⟨149::AID-HYP427⟩3.3.CO;2-F

Smith, R. (1983). Approximate soil water movement by kinematic characteristics. *Soil Science Society of America Journal*, *47*(1), 3–8. https://doi.org/10.2136/sssaj1983.03615995004700010001x

Stevens, C. M., Verjans, V., Lundin, J., Kahle, E. C., Horlings, A. N., Horlings, B. I., & Waddington, E. D. (2020). The community firn model (cfm) v1. 0. *Geoscientific Model Development*, *13*(9), 4355–4377. https://doi.org/10.5194/gmd-13-4355-2020

Team-IMBIE. (2018). Mass balance of the Antarctic ice sheet from 1992 to 2017. *Nature*, *558*(7709), 219–222. https://doi.org/10.1038/s41586-018-0179-y

Van Angelen, J. H., Lenaerts, J. T., Van Den Broeke, M. R., Fettweis, X., & Van Meijgaard, E. (2013). Rapid loss of firn pore space accelerates 21st century Greenland mass loss. *Geophysical Research Letters*, *40*(10), 2109–2113. https://doi.org/10.1002/grl.50490

Vandecrux, B., Mottram, R., Langen, P. L., Fausto, R. S., Olesen, M., Stevens, C. M., et al. (2020). The firn meltwater retention model intercomparison project (RETMIP): Evaluation of nine firn models at four weather station sites on the Greenland ice sheet. *The Cryosphere*, *14*(11), 3785–3810. https://doi.org/10.5194/tc-14-3785-2020

Van den Broeke, M., Bamber, J., Ettema, J., Rignot, E., Schrama, E., van de Berg, W. J., et al. (2009). Partitioning recent Greenland mass loss. *Science*, *326*(5955), 984–986. https://doi.org/10.1126/science.1178176

Velicogna, I., Mohajerani, Y., Geruo, A., Landerer, F., Mouginot, J., Noel, B., et al. (2020). Continuity of ice sheet mass loss in Greenland and Antarctica from the GRACE and GRACE follow-on missions. *Geophysical Research Letters*, *47*(8), e2020GL087291. https://doi.org/10.1029/2020GL087291

Wever, N., Würzer, S., Fierz, C., & Lehning, M. (2016). Simulating ice layer formation under the presence of preferential flow in layered snowpacks. *The Cryosphere*, *10*(6), 2731–2744. https://doi.org/10.5194/tc-10-2731-2016

Yao, T., & Hendrickx, J. M. H. (1996). Stability of wetting fronts in dry homogeneous soils under low infiltration rates. *Soil Science Society of America Journal*, *60*(1), 20–28. https://doi.org/10.2136/sssaj1996.03615995006000010006x

Yen, Y.-C. (1981). *Review of thermal properties of snow, ice, and sea ice* (Vol. 81(10)). US Army, Corps of Engineers, Cold Regions Research and Engineering Laboratory.

Zemp, M., Huss, M., Thibert, E., Eckert, N., McNabb, R., Huber, J., et al. (2019). Global glacier mass changes and their contributions to sea-level rise from 1961 to 2016. *Nature*, *568*(7752), 382–386. https://doi.org/10.1038/s41586-019-1071-0